Research Square

Preprints are preliminary reports that have not undergone peer review.
They should not be considered conclusive, used to inform clinical practice,
or referenced by the media as validated information.

A Multi-Feature Quality-Aware Gateway for Reliable Bidirectional HF–VHF/UHF Interoperability

PRABIR BANERJEE

prabir.banerjee@gmail.com

Heritage Institute of Technology https://orcid.org/0000-0001-8198-1397

Sabyasachi Chatterjee

Heritage Institute of Technology

Research Article

Keywords: HF–VHF/UHF interoperability, cross-band gateway, HF link-quality estimation, SINAD calibration, intelligent gateway arbitration, impulsive-noise mitigation

Posted Date: November 10th, 2026

DOI: https://doi.org/10.21203/rs.3.rs-11659019/v1

License: This work is licensed under a Creative Commons Attribution 4.0 International License.
Read Full License

Additional Declarations: The authors declare no competing interests.

A Multi-Feature Quality-Aware Gateway for Reliable Bidirectional HF–VHF/UHF Interoperability

Prabir Banerjee, Sabyasachi Chatterjee
ECE Department
Heritage Institute of Technology, Kolkata

Abstract
Achieving reliable interoperability between high-frequency (HF) and VHF/UHF communication systems presents significant challenges. Conventional VHF/UHF receivers offer stable squelch and carrier-operated-relay (COR) indications, while HF amplitude-modulated links are highly susceptible to background noise, fading, impulsive interference, and inaccurate received-energy measurements. This study introduces a quality-aware, bidirectional HF–VHF/UHF gateway that assesses communication usability rather than relying solely on carrier presence. The HF estimator integrates AGC/RSSI data, speech-band and noise-band energies, speech-likeness, and fading-instability features to produce a 0–5 V analog quality output and a hysteresis-controlled validity decision. The corresponding VHF/UHF estimator combines COR, RSSI, and audio-quality metrics. Both estimators are managed by a supervisory controller that implements first-valid-arrival arbitration, half-duplex enforcement, anti-loop lockout, attack/release timing, PTT pre-keying, and directional audio gating. A mathematical model and multi-stage simulation framework support HF signal recovery, feature extraction, quality-voltage generation, SINAD calibration, channel-impairment modeling, and gateway-state control. Across variations in SNR, fading, impulsive noise, heterodyne interference, and bidirectional contention, the proposed multi-feature method achieved a detection probability of 0.965, a false-open probability of 6.2×10^{-4}, a SINAD-calibration RMSE of 1.42 dB, and a gateway-arbitration success rate of 98.3%, with a mean response time of 42 ± 8 ms. These findings demonstrate that the architecture effectively suppresses noise-induced retransmission and enables stable cross-band operation, establishing a practical foundation for hybrid analog–digital gateways in emergency, field, and remote-area communication networks.

Keywords: HF–VHF/UHF interoperability; cross-band gateway; HF link-quality estimation; SINAD calibration; intelligent gateway arbitration; impulsive-noise mitigation.

I Introduction

Reliable interoperability between high-frequency (HF) and very-high-frequency/ultra-high-frequency (VHF/UHF) radio networks is critical for military, emergency-response, aviation, maritime, disaster-management, and remote-area communication systems. HF links enable long-range, beyond-line-of-sight connectivity via ionospheric propagation, eliminating the need for satellite infrastructure or extensive terrestrial repeater networks. In contrast, VHF/UHF systems typically offer more stable short-range and regional communication and can be easily integrated into repeater-based networks. Cross-band gateways that connect these radio domains can extend operational coverage, interconnect heterogeneous communication infrastructures, and allow users on otherwise incompatible radio systems to exchange voice information. However, reliable HF–VHF/UHF interfacing presents significant technical challenges due to fundamentally different receiver characteristics and signal-validation mechanisms [1], [2], [3]. The VHF/UHF frequency modulation (FM) or phase modulation (PM) receivers examined in this study benefit from the noise-quieting property of angle modulation, providing relatively dependable squelch and Carrier Operated Relay (COR) outputs. In contrast, an HF amplitude-modulated voice receiver does not offer an equivalent indication of communication usability [4],[5]. Atmospheric noise, impulsive electrical disturbances, selective fading, multipath propagation, heterodyne interference, and adjacent-channel activity can generate substantial received energy even when the recovered audio is severely distorted or unintelligible [7]. Automatic Gain Control (AGC) and Received Signal Strength Indicator (RSSI) measurements indicate the presence of energy but do not necessarily confirm that the received HF communication is suitable for retransmission. Forwarding such degraded audio directly into a VHF/UHF network can result in false transmitter keying, propagation of noise through repeaters, repeated gateway triggering, unnecessary channel occupation, and unstable bidirectional operation.

Modern high-frequency (HF) systems utilize Automatic Link Establishment, adaptive frequency management, and standardized networking protocols to enhance link availability. Previous research and standards have addressed HF interoperability and robust voice activity recognition [10], [21], [22]. However, carrier detection, automatic gain control (AGC) thresholding, voice-operated exchange (VOX) activation, fixed audio-level gating, and manual operator intervention are insufficient as stand-alone gateway-control mechanisms in highly variable HF environments. Furthermore, voice-activity detection alone does not address additional

challenges associated with bidirectional cross-band operation, such as simultaneous activity, retransmission loops, directional ownership, push-to-talk (PTT) coordination, and transition lockout. To the authors' knowledge, a comprehensive gateway framework that simultaneously evaluates HF voice-link usability, generates a hardware-compatible quality indication, and manages reliable bidirectional HF–VHF/UHF forwarding has not been adequately developed. This combined signal-quality and gateway-control issue represents the primary research gap addressed in this study. Consequently, an intelligent HF-validity estimation mechanism that assesses actual communication usability, rather than merely received energy, is necessary for stable cross-band interoperability

Reliable analog voice interoperability between HF and VHF/UHF radio networks is achieved through the development of a quality-aware bidirectional gateway architecture. In this system, recovered HF audio and AGC/RSSI measurements are conditioned and processed via parallel feature-extraction paths. Key features, including speech-band energy, high-frequency noise-band energy, speech-likeness characteristics, and fading-instability indicators, are estimated and combined using a weighted quality estimator to generate a bounded analog HF quality voltage. This voltage is converted into a stable digital HF-validity signal through the application of hysteresis, attack/release timing, and hang-time logic. Simultaneously, the VHF/UHF side is evaluated using COR, RSSI, speech-band energy, and noise-related measurements to produce a corresponding validity signal. The validity outputs from both HF and VHF/UHF are provided to a supervisory gateway controller, which manages first-valid-arrival arbitration, half-duplex enforcement, anti-loop lockout, PTT pre-keying, release timing, and directional audio-gate control. A mathematical model is formulated to describe the received signals, feature detectors, quality estimation, validity decisions, gateway-state transitions, audio gating, and PTT operation. The HF quality voltage is calibrated against reference SINAD to establish practical opening and closing thresholds. A multi-stage simulation framework is then employed to evaluate the proposed gateway under conditions such as fading, impulsive noise, heterodyne interference, speech activity, bidirectional contention, and timing scenarios. This is followed by the development of a hybrid analog–digital hardware realisation strategy, incorporating analog detector circuits, MCU-based supervisory control, isolated audio paths, and transmitter-interface circuitry.

The principal contributions of this study are outlined below:

1. A quality-aware, bidirectional HF–VHF/UHF gateway architecture is presented to enable reliable cross-band analog voice interoperability.
2. A multi-feature HF quality-estimation framework is developed, integrating AGC/RSSI, speech-band energy, noise-band energy, speech-likeness, and fading-instability metrics to assess communication usability beyond received energy alone.
3. An analog HF quality-voltage generation and SINAD-oriented calibration framework is introduced to facilitate practical gateway threshold selection and hardware implementation.
4. An intelligent gateway controller is developed, incorporating first-valid-arrival arbitration, anti-loop lockout, attack/release timing, half-duplex management, audio gating, and PTT coordination. This controller is evaluated using mathematical modelling and multi-stage simulation.

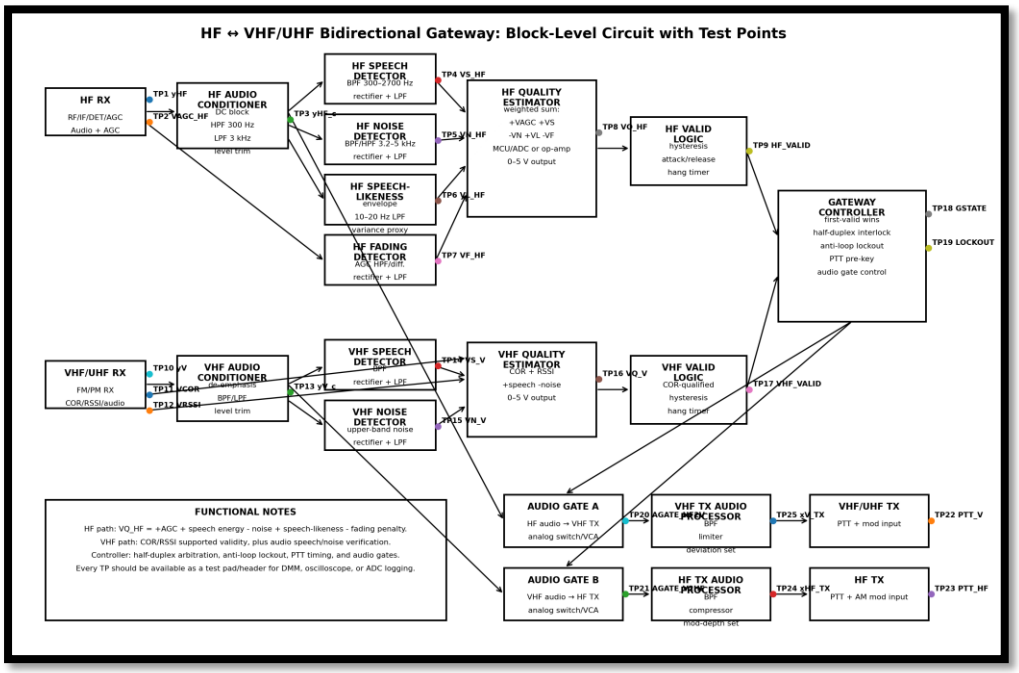


Fig. 1: Block Diagram of the entire scheme

1.4 Main Contributions

The principal contributions of this work are summarised as follows:

1. A novel quality-aware HF–VHF/UHF bidirectional gateway architecture is proposed for reliable cross-band interoperability.
2. A multi-feature HF quality-estimation framework combining AGC/RSSI measurements, speech-band energy, noise-band energy, speech-likeness metrics, and fading-instability indicators is developed.
3. An analogue HF quality voltage generation mechanism suitable for practical hardware realisation and gateway control is introduced.
4. A SINAD-oriented calibration framework for mapping the generated HF quality voltage to practical communication usability metrics is proposed.
5. An intelligent gateway controller implementing first-valid-arrival arbitration, anti-loop lockout, attack/release timing, and half-duplex management is designed.
6. A detailed mathematical model, including signal equations, detector equations, quality-estimation equations, and gateway-state equations, is developed.
7. A multi-stage simulation framework supporting fading, impulsive noise, interference, arbitration scenarios, and gateway timing analysis is implemented and evaluated.
8. A practical hardware realization strategy including analog detector blocks, MCU-based supervisory control, audio gating, and PTT interfacing is presented.

Table 1: Comparison of Conventional and Proposed HF–VHF/UHF Gateway Architectures

Existing Method	RSSI	VOX	COR	Multi-feature	Arbitration	Analog Quality Voltage
Conventional gateway	✓	✓	✗	✗	✗	✗
Proposed gateway	✓	✓	✓	✓	✓	✓

A comparison of the proposed HF–VHF/UHF gateway with a conventional gateway is presented in Table 1. The proposed architecture integrates COR, multi-feature quality estimation, gateway arbitration, and an analog quality-voltage output in addition to RSSI and VOX.

1.5 Organization of the Paper

The remainder of this paper is organized as follows. Section 2 discusses the background characteristics of HF and VHF/UHF communication systems and the limitations of existing interoperability approaches. Section 3 presents the proposed gateway architecture and associated functional blocks. Section 4 develops the mathematical formulation of the proposed system including quality-estimation and gateway-control equations. Section 5 describes the simulation framework and calibration methodology. Section 6 presents simulation results and performance analysis under varying channel conditions. Section 7 discusses practical hardware realization aspects and implementation considerations. Finally, Section 8 concludes the paper and outlines future research directions.

2. Background and Motivation

2.1 Characteristics of HF Communication Systems

High Frequency (HF) communication systems operating in the (3–30) MHz frequency range remain highly important for long-distance beyond-line-of-sight communication due to their ability to exploit ionospheric propagation. Unlike terrestrial line-of-sight communication systems, HF links can support intercontinental communication without reliance on satellite infrastructure or extensive repeater networks. Consequently, HF systems continue to play important roles in aviation, maritime communication, defense communication, emergency response, remote-area connectivity, and disaster-management applications [7], [8].

Despite these advantages, HF communication links are inherently difficult to stabilize because the propagation medium is highly variable. HF signals are strongly affected by ionospheric variability, multipath propagation, selective fading, Doppler spread, atmospheric noise, impulsive interference, man-made electrical noise, adjacent-channel interference, and heterodyne tones. As a result, the recovered audio quality in HF systems may fluctuate significantly even when substantial received energy is present at the receiver input. In conventional AM-based HF receivers, the Automatic Gain Control (AGC) mechanism responds primarily to received signal amplitude rather than recovered speech intelligibility. Therefore, strong AGC or RSSI indications do not necessarily imply usable communication quality.

.

2.2 Characteristics of VHF/UHF FM Communication Systems

VHF and UHF communication systems operating with frequency modulation or phase modulation exhibit significantly different receiver behavior compared to HF AM systems. FM communication receivers benefit from the well-known noise quieting phenomenon, whereby high-frequency discriminator noise decreases rapidly once a valid carrier exceeds the receiver threshold. This behavior enables highly effective implementation of noise-operated squelch, Carrier Operated Relay (COR), Received Signal Strength Indicator (RSSI)-based validation, repeater keying logic, and automatic channel access control [11],[12].

However, when HF communication systems are directly interfaced with VHF/UHF systems using conventional gateway techniques, the mismatch between HF and FM receiver behavior becomes problematic. The VHF/UHF side expects stable and meaningful validity indications, whereas the HF side often produces noisy and ambiguous signal conditions. This mismatch constitutes the central interoperability challenge addressed in this work [13].

2.3 Challenges in HF–VHF/UHF Interoperability

Reliable interoperability between HF and VHF/UHF communication systems requires stable and accurate determination of whether the received HF signal is suitable for retransmission into the VHF/UHF network. Several challenges arise in this context. Unlike FM systems, HF AM receivers do not exhibit strong noise quieting characteristics. Consequently, conventional squelch circuits based on noise reduction are generally unreliable in HF environments. High atmospheric noise and fading frequently produce situations in which AGC voltage is high, received energy appears substantial, but recovered speech intelligibility remains poor. This makes simple threshold-based gating ineffective.

HF signals often experience rapid amplitude fluctuations due to multipath propagation and ionospheric variability. Even when speech is initially intelligible, sudden fading events may temporarily degrade communication quality below usable levels. If gateway control logic responds too aggressively to these fluctuations, unstable retransmission and repeated gateway triggering may occur [21], [22].

Therefore, robust gateway operation requires attack/release control, hysteresis, hang-time management, and fading-aware validity estimation [9], [10].

HF communication channels are frequently contaminated by lightning-induced atmospheric noise, impulsive electrical interference, switching noise, and broadband impulsive disturbances. Such noise components may trigger conventional VOX or energy-based gateway circuits even in the absence of meaningful communication content [14], [15].

In bidirectional interoperability systems, another major challenge is the prevention of retransmission loops. If retransmitted audio from one side re-enters the opposite receiver chain, uncontrolled repeated gateway triggering may occur. This problem becomes particularly severe when both communication sides become simultaneously active, gateway release timing is poorly controlled, or audio leakage/acoustic coupling exists.

Consequently, practical interoperability systems require directional arbitration, lockout logic, half-duplex enforcement, and controlled release timing [16].

2.4 Limitations of Existing Gateway Approaches

Existing analogue gateway systems often rely on relatively simple gating approaches, including VOX-based activation, AGC-threshold triggering, fixed audio-level comparators, manual operator intervention, and carrier-only detection [17], [18], [19].

Although such methods may function under controlled conditions, they typically perform poorly in realistic HF environments.

These limitations motivate the development of a quality-aware gateway architecture capable of estimating actual communication usability rather than merely indicating the presence of an HF signal [2],[3],[4] [20].

3. Proposed System Architecture

3.1 Overview of the Proposed Gateway

The proposed system is a quality-aware bidirectional HF–VHF/UHF gateway designed to provide reliable interoperability between noisy HF communication links and comparatively stable VHF/UHF FM communication systems. The gateway operates as a controlled half-duplex communication bridge in which intelligent signal validity estimation determines whether communication should be forwarded between the two radio domains [24], [25].

The gateway consists of four principal subsystems:

1. HF receive-quality estimation subsystem,
2. VHF/UHF receive-validity estimation subsystem,
3. Gateway control and arbitration subsystem,
4. Audio gating and transmitter interface subsystem.

A complete block-level architecture of the proposed gateway is shown in Fig. 1.

3.2 HF Receive-Quality Estimation Subsystem

The HF receive-quality estimation subsystem constitutes the most important component of the proposed architecture. Its objective is to estimate actual communication usability rather than simply detecting received RF energy.

The subsystem accepts recovered HF audio, AGC/RSSI-related measurements, and envelope stability information from the HF receiver.

The conditioned audio is then processed through multiple parallel feature-extraction paths. The conditioned audio is then processed through multiple parallel feature-extraction paths. Fig. 2 shows the block diagram of the estimator for the HF multi-feature scheme. In Fig. 1, which represents the complete block diagram of the interfacing system, TP23 is the PTT_HF signal. In Fig. 2, TP10 is the "HF Validity Output/V_{HF_VALID} command output.

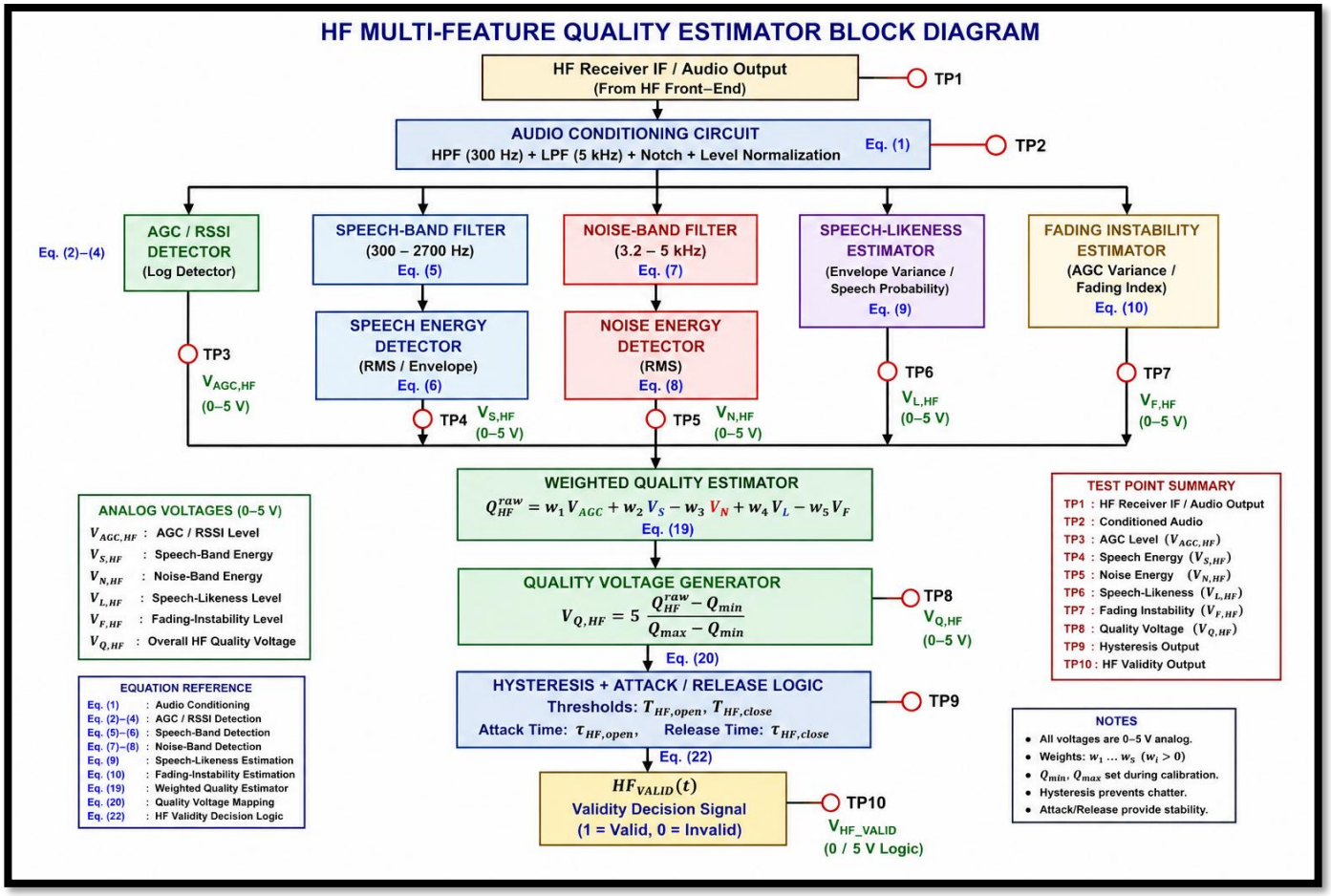


Fig. 2: Estimator Block Diagram for the HF-VHF Interfacing Scheme

The first feature-extraction path estimates the useful speech-band energy. The conditioned HF audio is passed through a band-pass filter covering approximately 300 Hz to 2700/3000 Hz, corresponding to the primary communication speech band. The filtered output is rectified and low-pass filtered to generate a speech-energy-related voltage proportional to the short-time speech-band power.
This feature provides information regarding the amount of potentially useful communication content present in the received audio.
The second feature-extraction path estimates post-detection noise energy. A high-frequency band-pass or high-pass filter is used to isolate predominantly noise-dominated spectral regions, typically between approximately 3.2 kHz and 5 kHz. The filtered signal is rectified and smoothed to generate a noise-related voltage.
This feature is important because excessive post-detection noise indicates poor communication quality even if strong RF energy is present.
The third feature-extraction path estimates speech-likeness behaviour. Human speech exhibits characteristic syllabic envelope variations at comparatively low modulation rates. To exploit this property, the speech-band signal envelope is extracted and low-pass filtered at syllabic rates. The resulting envelope fluctuations are processed to estimate speech-likeness behaviour.
This feature helps suppress false gateway activation caused by stationary noise, heterodyne tones, and non-speech interference.
The fourth feature-extraction path estimates fading instability. Rapid fluctuations in AGC or received-envelope measurements are characteristic of unstable HF fading conditions. By measuring short-time variance or instability of AGC-derived quantities, the gateway estimates whether the HF channel is sufficiently stable for retransmission.
The resulting fading-instability metric acts as a penalty term in the quality estimator.
The extracted features are combined through a weighted quality estimator to generate an analogue HF quality voltage and a binary HF-validity signal.
The analogue quality voltage provides hardware observability, threshold calibration capability, and practical gateway-control support.
The binary validity signal is produced using hysteresis-based attack/release logic with hang-time support to prevent unstable gateway behavior under fading conditions.

3.3 VHF/UHF Receive-Validity Estimation Subsystem

The VHF/UHF receive-validity subsystem is comparatively simpler because FM communication systems already provide reliable COR and squelch behaviour. The subsystem processes COR/squelch outputs, RSSI measurements, and recovered VHF/UHF audio.
The received audio is conditioned through filtering and level normalisation stages. Speech-band and optional noise-band measurements are then extracted.
A validity estimator combines COR state, RSSI level, speech-band energy, and noise-related measurements to generate a VHF/UHF quality voltage and a VHF/UHF validity signal.
This signal is subsequently used by the gateway controller for arbitration and retransmission decisions.

3.4 Gateway Control and Arbitration Subsystem

The gateway controller coordinates all cross-band communication activities. The proposed architecture employs first-valid-arrival arbitration, half-duplex enforcement, anti-loop lockout, hang-time management, attack/release timing, and transmitter keying control.
At any instant, the gateway operates in one of four states:

1. idle,
2. HF-to-VHF/UHF active,
3. VHF/UHF-to-HF active,
4. lockout/transition state.

When one communication direction becomes active, the opposite direction is temporarily inhibited to prevent gateway looping and unstable bidirectional retransmission.
The controller further manages PTT pre-key timing, audio-gate activation, release timing, and retransmission lockout intervals.

3.5 Audio Gating and Transmitter Interface Subsystem

The gateway contains two independently controlled audio paths:

1. HF receive audio to the VHF/UHF transmitter,
2. VHF/UHF receive audio to HF transmitter.

Each path contains analogue audio gating, level conditioning, limiter/compressor stages, and transmitter-specific audio processing.
The HF transmitter path additionally includes modulation-depth control to prevent overmodulation. The VHF/UHF path includes deviation-limiting circuitry to maintain acceptable FM deviation levels.
Audio gates are controlled by the gateway controller and operate only when the corresponding gateway state is active.

3.6 Hardware Realisation Strategy

The proposed architecture is intended for practical realisation using a hybrid analogue-digital approach. Analogue front-end detector circuits generate the required feature voltages, while a microcontroller-based supervisory controller performs quality estimation, validity logic, arbitration, lockout control, PTT management, and optional quality-voltage calibration.
The architecture also exposes multiple test points corresponding to detector outputs, quality voltages, logic states, and PTT signals to facilitate calibration and laboratory evaluation.

3.7 Advantages of the Proposed Architecture

The proposed gateway architecture offers several advantages over conventional cross-band gateway systems:

1. HF communication usability is estimated using multiple signal features rather than single-threshold detection.
2. The architecture supports robust operation under fading and impulsive-noise conditions.
3. The generated HF quality voltage provides practical calibration capability.
4. Intelligent arbitration and anti-loop control improve bidirectional stability.
5. The architecture is compatible with both analogue and MCU-assisted hardware realisation approaches.
6. The modular structure supports future SDR and adaptive-threshold extensions.

The proposed architecture therefore, provides a practical and scalable framework for intelligent HF–VHF/UHF interoperability.

4. Mathematical Model

4. Mathematical Model

4.1 HF Received Signal and Demodulation Model

The radio frequency (RF) high-frequency (HF) amplitude-modulated (AM) signal arriving at the receiver antenna terminal is modeled as:

$$x_{\mathrm{HF}}(t) = a_{\mathrm{HF}}(t)[1 + \mu_{\mathrm{HF}}\, m_{\mathrm{HF}}(t)]\cos\left(2\pi f_{\mathrm{c,HF}} t + \varphi_{\mathrm{HF}}(t)\right) + n_{\mathrm{rf}}(t) + i_{\mathrm{HF}}(t) \text{ ----------} (1)$$

where:

- $a_{\mathrm{HF}}(t)$ represents the time-varying fading amplitude envelope.
- μ_{HF} is the modulation index ($0 < \mu_{\mathrm{HF}} \leq 1$).
- $m_{\mathrm{HF}}(t)$ is the normalized audio baseband speech message signal, bounded such that $\max|m_{\mathrm{HF}}(t)| \leq 1$.
- $f_{\mathrm{c,HF}}$ denotes the HF carrier frequency.
- $\varphi_{\mathrm{HF}}(t)$ is the phase perturbation introduced by ionospheric dispersion.
- $n_{\mathrm{rf}}(t)$ is the additive white Gaussian noise (AWGN) present at the RF front-end.
- $i_{\mathrm{HF}}(t)$ represents co-channel or adjacent-channel heterodyne interference.

Following envelope demodulation and audio stage amplification, the recovered raw baseband audio signal $y_{\mathrm{HF}}(t)$ is expressed as:

$$y_{\mathrm{HF}}(t) = K_{\mathrm{d,HF}}\, a_{\mathrm{HF}}(t)\, \mu_{\mathrm{HF}}\, m_{\mathrm{HF}}(t) + n_{\mathrm{a,HF}}(t) + d_{\mathrm{HF}}(t) + \eta_{\mathrm{HF}}(t) \text{ ---------- } (2)$$

where $K_{\mathrm{d,HF}}$ is the receiver detector gain constant, $n_{\mathrm{a,HF}}(t)$ is the demodulated baseband noise, $d_{\mathrm{HF}}(t)$ represents harmonic distortion products, and $\eta_{\mathrm{HF}}(t)$ is the residual post-detection impulsive noise component.

Applying the linear time-invariant (LTI) system approximation of the audio conditioning circuit, the pre-processed audio stream $y_{\mathrm{HF,c}}(t)$ yields:

$$y_{\mathrm{HF,c}}(t) = \mathcal{F}_{\mathrm{HF}}\{y_{\mathrm{HF}}(t)\} = G_{\mathrm{HF}} \int_{-\infty}^{\infty} h_{\mathrm{HF}}(\tau) y_{\mathrm{HF}}(t-\tau) d\tau \text{ ----------} (3)$$

where G_{HF} is the normalization gain and $h_{\mathrm{HF}}(t)$ represents the combined impulse response of the DC-blocking, high-pass, and notch filtering array.

4.2 HF Feature Extraction Estimators

4.2.1 Received Signal Strength and AGC Proxy Model

The Automatic Gain Control (AGC) or Received Signal Strength Indicator (RSSI) voltage is modeled as a short-time averaged energy detector operating over the intermediate frequency (IF) band:

$$V_{\mathrm{AGC,HF}}(t) = K_{\mathrm{AGC,HF}} \cdot \frac{1}{T_{\mathrm{AGC}}} \int_{t-T_{\mathrm{AGC}}}^{t} \left| x_{\mathrm{IF,HF}}(\tau) \right|^2 d\tau \text{ ----------(4)}$$

where $x_{\mathrm{IF,HF}}(t)$ is the pre-demodulated IF signal, T_{AGC} is the active tracking time window, and $K_{\mathrm{AGC,HF}}$ is a linear voltage scaling coefficient.

4.2.2 Speech-Band Energy Estimator

Let $h_{\mathrm{S,HF}}(t)$ define the impulse response of the primary speech band-pass filter (300–2700 Hz). The isolated speech-band component is derived via:

$$y_{\mathrm{S,HF}}(t) = h_{\mathrm{S,HF}}(t) * y_{\mathrm{HF,c}}(t) \text{ ----------(5)}$$

The short-time speech-band power $P_{\mathrm{S,HF}}(t)$ and its corresponding rectified analog voltage output $V_{\mathrm{S,HF}}(t)$ are formulated as:

$$\begin{aligned} P_{\mathrm{S,HF}}(t) &= \frac{1}{T_{\mathrm{S}}} \int_{t-T_{\mathrm{S}}}^{t} \left| y_{\mathrm{S,HF}}(\tau) \right|^2 d\tau \\ V_{\mathrm{S,HF}}(t) &= K_{\mathrm{S,HF}} \cdot \sqrt{P_{\mathrm{S,HF}}(t)} \end{aligned} \text{ ----------(6)}$$

where T_{S} is the speech integration window (40 ms) and $K_{\mathrm{S,HF}}$ is the detector scaling factor.

4.2.3 Noise-Band Energy Estimator

Let $h_{\mathrm{N,HF}}(t)$ define the impulse response of the high-frequency out-of-band filter (3.2–5.0 kHz). The isolated out-of-band noise component is extracted via:

$$y_{\mathrm{N,HF}}(t) = h_{\mathrm{N,HF}}(t) * y_{\mathrm{HF,c}}(t) \text{ ----------(7)}$$

The corresponding short-time noise-band power $P_{\mathrm{N,HF}}(t)$ and rectified analog voltage output $V_{\mathrm{N,HF}}(t)$ are modeled as:

$$\begin{aligned} P_{\mathrm{N,HF}}(t) &= \frac{1}{T_{\mathrm{N}}} \int_{t-T_{\mathrm{N}}}^{t} \left| y_{\mathrm{N,HF}}(\tau) \right|^2 d\tau \\ V_{\mathrm{N,HF}}(t) &= K_{\mathrm{N,HF}} \cdot \sqrt{P_{\mathrm{N,HF}}(t)} \end{aligned} \text{ ----------(8)}$$

where T_{N} is the rapid noise integration window (5 ms) and $K_{\mathrm{N,HF}}$ is the noise voltage calibration coefficient.

4.2.4 Speech-Likeness Level Estimator

The analytic envelope $e_{\mathrm{HF}}(t)$ of the speech-band signal is obtained using the Hilbert transform operator $\mathcal{H}\{\cdot\}$:

$$e_{\mathrm{HF}}(t) = \left| y_{\mathrm{S,HF}}(t) + j\mathcal{H}\{y_{\mathrm{S,HF}}(t)\} \right| \text{----------(9)}$$

The extracted envelope is filtered by the low-pass syllabic matrix $h_{\mathrm{L,HF}}(t)$ targeting 10–20 Hz frequencies:

$$\tilde{e}_{\mathrm{HF}}(t) = h_{\mathrm{L,HF}}(t) * e_{\mathrm{HF}}(t) \text{----------(10)}$$

The short-time envelope variance over a long-term processing window T_{L} (250 ms) establishes the variance proxy metric $\sigma^2_{\mathrm{e,HF}}(t)$:

$$\sigma^2_{\mathrm{e,HF}}(t) = \frac{1}{T_{\mathrm{L}}} \int_{t-T_{\mathrm{L}}}^{t} (\tilde{e}_{\mathrm{HF}}(\tau) - \mathbb{E}[\tilde{e}_{\mathrm{HF}}])^2 \, d\tau \text{----------(11)}$$

The dedicated speech-likeness validation voltage $V_{\mathrm{L,HF}}(t)$ is then derived by normalizing the variance proxy against the current out-of-band noise floor:

$$V_{\mathrm{L,HF}}(t) = K_{\mathrm{L,HF}} \cdot \frac{\sigma^2_{\mathrm{e,HF}}(t)}{P_{\mathrm{N,HF}}(t)+\epsilon} \text{----------(12)}$$

where ϵ is an infinitesimally small regularization constant preventing division-by-zero singularities, and $K_{\mathrm{L,HF}}$ is a linear scaling gain.

4.2.5 Fading Instability Estimator

Let $\sigma^2_{\mathrm{AGC,HF}}(t)$ denote the short-time variance of the absolute AGC voltage level, and $\sigma^2_{\mathrm{S,HF}}(t)$ define the short-time variance of the recovered speech voltage, both evaluated over a short fading window T_{F} (500 ms):

$$\begin{aligned} \sigma^2_{\mathrm{AGC,HF}}(t) &= \mathrm{Var}_{T_{\mathrm{F}}}\{V_{\mathrm{AGC,HF}}(t)\} \\ \sigma^2_{\mathrm{S,HF}}(t) &= \mathrm{Var}_{T_{\mathrm{F}}}\{V_{\mathrm{S,HF}}(t)\} \end{aligned} \text{----------(13)}$$

The composite analog fading instability penalty voltage $V_{\mathrm{F,HF}}(t)$ is mathematically combined as:

$$V_{\mathrm{F,HF}}(t) = K_{\mathrm{F,HF}}\left(\alpha_{\mathrm{F}}\,\sigma^2_{\mathrm{AGC,HF}}(t) + \beta_{\mathrm{F}}\,\sigma^2_{\mathrm{S,HF}}(t)\right) \text{----------(14)}$$

where α_{F} and β_{F} are relative weighting coefficients, and $K_{\mathrm{F,HF}}$ maps the variance directly to the 0–5 V hardware limit.

4.3 Multi-Feature Parametric Fusion and Hysteretic Gating Logic

The raw multi-feature quality estimation index $Q^{\mathrm{raw}}_{\mathrm{HF}}(t)$ fuses the five parallel metrics linearly:

$$Q^{\mathrm{raw}}_{\mathrm{HF}}(t) = w_1 V_{\mathrm{AGC,HF}}(t) + w_2 V_{\mathrm{S,HF}}(t) - w_3 V_{\mathrm{N,HF}}(t) + w_4 V_{\mathrm{L,HF}}(t) - w_5 V_{\mathrm{F,HF}}(t) \text{----------(15)}$$

where $w_1, \ldots, w_5 > 0$ represent the individual empirical tuning weights. This raw value is constrained to create the bounded analog diagnostic quality voltage $V_{\mathrm{Q,HF}}(t)$:

$$V_{\mathrm{Q,HF}}(t) = 5 \cdot \left[\frac{Q^{\mathrm{raw}}_{\mathrm{HF}}(t) - Q_{\min}}{Q_{\max} - Q_{\min}}\right] \text{----------(16)}$$

To evaluate signal stability, the system defines dual hysteretic boundaries where the opening threshold $T_{\mathrm{HF,open}}$ exceeds the closing threshold $T_{\mathrm{HF,close}}$:

$$T_{\mathrm{HF,open}} > T_{\mathrm{HF,close}} \text{----------(17)}$$

The final binary digital validity decision function $\mathrm{HF}_{\mathrm{VALID}}(t) \in \{0,1\}$ tracks state changes over time using explicit attack ($\tau_{\mathrm{HF,open}}$) and release ($\tau_{\mathrm{HF,close}}$) integration parameters:

$$\mathrm{HF}_{\mathrm{VALID}}(t) = \begin{cases} 1, & \text{if } V_{\mathrm{Q,HF}}(t) > T_{\mathrm{HF,open}} \ \wedge\ \Delta t > \tau_{\mathrm{HF,open}} \\ 0, & \text{if } V_{\mathrm{Q,HF}}(t) < T_{\mathrm{HF,close}} \ \wedge\ \Delta t > \tau_{\mathrm{HF,close}} \\ \mathrm{HF}_{\mathrm{VALID}}(t^-), & \text{otherwise} \end{cases} \text{----------(18)}$$

where $\mathrm{HF}_{\mathrm{VALID}}(t^-)$ maintains the historical logic state execution state to suppress transition chatter.

4.4 VHF/UHF Link Validity Formulation

The input signal vector entering the VHF/UHF frequency modulation (FM) receiver is modeled as:

$$x_{\mathrm{V}}(t) = a_{\mathrm{V}}(t)s_{\mathrm{V}}(t) + n_{\mathrm{V}}(t) + i_{\mathrm{V}}(t) \text{----------(19)}$$

where $a_{\mathrm{V}}(t)$ is a stable local attenuation path vector, $s_{\mathrm{V}}(t)$ represents the phase/frequency modulated transmission, $n_{\mathrm{V}}(t)$ denotes the quieted discriminator noise component, and $i_{\mathrm{V}}(t)$ is local interference.

The raw quality index for the VHF domain $Q_{\mathrm{V}}(t)$ combines the physical Carrier Operated Relay (V_{COR}) status with the RSSI metrics and baseband speech indicators:

$$Q_{\mathrm{V}}(t) = u_1 V_{\mathrm{COR}}(t) + u_2 V_{\mathrm{RSSI,V}}(t) + u_3 V_{\mathrm{S,V}}(t) - u_4 V_{\mathrm{N,V}}(t) \text{----------(20)}$$

where $u_1, \ldots, u_4$ represent the specific processing weights. The resulting digital state function $\mathrm{VHF}_{\mathrm{VALID}}(t)$ is evaluated as:

$$\mathrm{VHF}_{\mathrm{VALID}}(t)=\begin{cases}1, & \text{if } Q_{\mathrm{V}}(t)>T_{\mathrm{V,open}}\\ 0, & \text{if } Q_{\mathrm{V}}(t)<T_{\mathrm{V,close}}\\ \mathrm{VHF}_{\mathrm{VALID}}(t^{-}), & \text{otherwise}\end{cases}\text{----------(21)}$$

4.5 Supervisory Architecture Control States

The supervisory logic controller defines a finite state machine tracking a global state index $\mathrm{GSTATE}(t)$:

$$\mathrm{GSTATE}(t)\in\{0,1,2,3\}\text{----------(22)}$$

where:

- $\mathrm{GSTATE}=0$: System Idle/Monitor state.
- $\mathrm{GSTATE}=1$: HF-to-VHF/UHF Forwarding active.
- $\mathrm{GSTATE}=2$: VHF/UHF-to-HF Forwarding active.
- $\mathrm{GSTATE}=3$: Anti-loop Lockout/Transition state.

The active state-switching transitions for forwarding voice are driven by the logical interlocks:

$$\begin{aligned}\mathrm{GSTATE}(t)=1 \quad \text{if} \quad \mathrm{HF}_{\mathrm{VALID}}(t)=1\ \wedge\ \mathrm{GSTATE}(t^{-})=0\\ \mathrm{GSTATE}(t)=2 \quad \text{if} \quad \mathrm{VHF}_{\mathrm{VALID}}(t)=1\ \wedge\ \mathrm{GSTATE}(t^{-})=0\end{aligned}\text{----------(23)}$$

The solid-state linear audio gate control drivers ($\mathrm{AGATE}_{\mathrm{HF\to V}}$ and $\mathrm{AGATE}_{\mathrm{V\to HF}}$) execute binary transparency routing according to:

$$\begin{aligned}\mathrm{AGATE}_{\mathrm{HF\to V}}(t)&=\begin{cases}1, & \text{if } \mathrm{GSTATE}(t)=1\\ 0, & \text{otherwise}\end{cases}\\ \mathrm{AGATE}_{\mathrm{V\to HF}}(t)&=\begin{cases}1, & \text{if } \mathrm{GSTATE}(t)=2\\ 0, & \text{otherwise}\end{cases}\end{aligned}\text{----------(24)}$$

The hardware transceiver PTT command output lines are controlled by shifting the active timing window backwards by an explicit pre-key delay interval τ_{pre}:

$$\mathrm{PTT}_{\mathrm{V}}(t)=\mathrm{AGATE}_{\mathrm{HF\to V}}(t-\tau_{\mathrm{pre}})\text{----------(25)}$$

$$\mathrm{PTT}_{\mathrm{HF}}(t)=\mathrm{AGATE}_{\mathrm{V\to HF}}(t-\tau_{\mathrm{pre}})\text{----------(26)}$$

4.6 SINAD Calibration Model Formulation

To calibrate the absolute generated hardware voltage tracking indicator $V_{\mathrm{Q,HF}}$ back to standard communication readability criteria, the true reference Signal-to-Noise and Distortion (SINAD) ratio is calculated:

$$\mathrm{SINAD}_{\mathrm{HF}}(t)=10\log_{10}\left[\frac{P_{\mathrm{S}}(t)+P_{\mathrm{N+D}}(t)}{P_{\mathrm{N+D}}(t)}\right]\text{----------(27)}$$

where $P_{\mathrm{S}}(t)$ is the verified clean baseband reference signal power, and $P_{\mathrm{N+D}}(t)$ defines the total combined noise-plus-distortion remainder power tracking vector. The empirical conversion mapping function is estimated via polynomial regression:

$$\mathrm{SINAD}_{\mathrm{HF}}\approx a_0+a_1V_{\mathrm{Q,HF}}+a_2V_{\mathrm{Q,HF}}^2\text{----------(28)}$$

where a_0, a_1, and a_2 represent the empirical calibration coefficients established during laboratory environmental characterization loops.

4.7 Frame-Wise Discrete-Time Transformation

For discrete-time algorithmic execution within the microcontroller firmware, continuous waveforms are segmented into uniform frames index k consisting of N distinct samples spaced by a sampling period $T_{\mathrm{s}}=1/f_{\mathrm{s}}$.

The frame-wise signal power parameters are computed as:

$$P_{\mathrm{S,HF}}[k] = \frac{1}{N}\sum_{n=0}^{N-1}\left|y_{\mathrm{S,HF}}[kN+n]\right|^2$$
$$P_{\mathrm{N,HF}}[k] = \frac{1}{N}\sum_{n=0}^{N-1}\left|y_{\mathrm{N,HF}}[kN+n]\right|^2 \text{----------(29)}$$

The discrete tracking operations executed at each time step loop are denoted via:

$$V_{\mathrm{Q,HF}}[k] = \mathcal{Q}\{V_{\mathrm{AGC,HF}}[k],\ V_{\mathrm{S,HF}}[k],\ V_{\mathrm{N,HF}}[k],\ V_{\mathrm{L,HF}}[k],\ V_{\mathrm{F,HF}}[k]\}$$
$$\mathrm{GSTATE}[k] = \mathcal{G}\{\mathrm{HF}_{\mathrm{VALID}}[k],\ \mathrm{VHF}_{\mathrm{VALID}}[k],\ \mathrm{LOCKOUT}[k]\} \text{----------(30)}$$

where $\mathcal{Q}\{\cdot\}$ represents the non-linear multi-feature fusion operator and $\mathcal{G}\{\cdot\}$ represents the sequential logic gate state transition operator.

Simulation Framework and Calibration Methodology

5.1 Overview of the Simulation Framework

A multi-stage simulation framework was developed to evaluate the proposed quality-aware HF–VHF/UHF gateway architecture under realistic communication conditions. The simulation environment was designed to investigate HF quality-voltage behavior, validity-detection performance, fading robustness, impulsive-noise tolerance, gateway arbitration behaviour, lockout stability, and SINAD-oriented calibration characteristics.

The simulation framework evolved through multiple stages:

1. preliminary HF quality estimation,
2. bidirectional gateway simulation,
3. gateway-state analysis,
4. explicit $V_{Q,HF}$-to-SINAD calibration.

The simulations were implemented in Python and Matplotlib.

5.2 HF Communication Signal Generation

The HF communication signal was modeled as an amplitude-modulated communication waveform carrying synthetic speech-like baseband content.

The baseband communication signal consisted of multiple voice-like sinusoidal components, speech-band filtering, syllabic envelope modulation, and active speech intervals separated by pauses.

The resulting normalized baseband speech signal $m_{HF}(t)$was used to generate the transmitted AM waveform according to:

$$x_{HF(t)} = \left[1 + \mu_{HF} m_{HF(t)}\right]\cos(2\pi\, f_c, HF\ t) - - - \quad (39)$$

where:

- $f_{c,HF}$denotes the HF carrier frequency,
- μ_{HF}denotes the modulation index.

The simulation framework allowed controlled variation of modulation depth, speech activity, and communication burst timing.

5.3 HF Channel Modeling

Additive White Gaussian Noise (AWGN) was introduced to emulate background channel noise:

$$x_{HF}, n(t) = x_{HF(t)} + n_{HF(t)} - - - - - \ (40)$$

where:

- $n_{HF}(t)$is Gaussian-distributed noise.

The simulations considered a wide range of HF SNR values to evaluate gateway performance under weak and noisy communication conditions.

HF Fading Model

To emulate ionospheric fading behavior, a composite fading envelope was introduced:

$$a_{HF(t)} = 1 + \Sigma_{i=1}^{M}\alpha_i \sin(2\pi\, f_i t + \theta_i) - - - \ (41)$$

where:

- $\alpha_i$are fading amplitudes,
- $f_i$are fading frequencies,
- $\theta_i$are random phases.

The fading envelope was clipped to avoid physically unrealistic negative amplitudes.
The fading model allowed controlled variation of fading depth, fading rate, and instability severity.

Impulsive Noise Model
Impulsive noise events were introduced probabilistically:

$$x_{HF}, imp(t) = x_{HF(t)} + \eta_{imp(t)} ---- (42)$$

where:

- $\eta_{imp}(t)$represents randomly occurring impulsive disturbances.

The impulsive-noise model simulated atmospheric bursts, electrical switching noise, and transient interference.

Interference Modeling
Sinusoidal heterodyne interference was introduced using:

$$i_{HF(t)} = A_i \cos(2\pi f_i t) ---- (43)$$

where:

- $A_i$denotes interference amplitude,
- $f_i$denotes heterodyne frequency.

This enabled evaluation of the gateway under adjacent-channel interference conditions.

5.4 HF Receiver and Audio Recovery Simulation
The HF receiver model consisted of envelope detection, audio recovery, high-pass filtering, low-pass filtering, and audio conditioning.
The recovered audio was represented as:

$$y_{HF}(t) = \mathcal{R}_{HF}\{x_{HF}(t)\} ---------- (44)$$

where $\mathcal{R}_{HF}\{\cdot\}$denotes the receiver operation.
The conditioned audio was subsequently used for:

- speech-band estimation,
- noise-band estimation,
- speech-likeness analysis,
- and fading-instability estimation.

5.5 HF Feature Extraction and Quality Estimation
For each simulation frame, the following quantities were computed:

- AGC/RSSI proxy:

$$V_{AGC,HF}[k]$$

- speech-band detector output:

$$V_{S,HF}[k]$$

- noise-band detector output:

$$V_{N,HF}[k]$$

- speech-likeness detector output:

$$V_{L,HF}[k]$$

- fading-instability detector output:

$$V_{F,HF}[k]$$

The frame-wise quality score was then generated according to:

$$Q_{HF}[k] = w_1 V_{AGC,HF}[k] + w_2 V_{S,HF}[k] - w_3 V_{N,HF}[k] + w_4 V_{L,HF}[k] - w_5 V_{F,HF}[k] \quad ----------(45)$$

The resulting quantity was normalized to generate the analog quality voltage:

$$V_{Q,HF}[k] \in [0,5] \text{ V} \quad ---------- \quad (46)$$

5.6 VHF/UHF Communication Modeling

The VHF/UHF side was modeled using audio-domain communication generation, FM/PM-like audio recovery behavior, RSSI proxy generation, and COR-like validity logic.

Compared to HF, the VHF/UHF side operated under comparatively stable channel conditions, reduced fading severity, and lower impulsive-noise sensitivity.

The VHF validity estimator combined COR state, RSSI, speech-band power, and noise-band power.

5.7 Bidirectional Gateway Simulation

The gateway simulator implemented HF-to-VHF communication forwarding, VHF-to-HF communication forwarding, first-valid-arrival arbitration, anti-loop lockout, half-duplex enforcement, PTT pre-key timing, and audio-gate activation [31].

The simulation supported multiple gateway scenarios, including HF-first communication activity, VHF-first communication activity, simultaneous activity contention, and noise-stressed operation.

The gateway controller produced gateway-state outputs, PTT signals, lockout indicators, and audio-gate activation states. Fig. 3 shows the gateway connections.

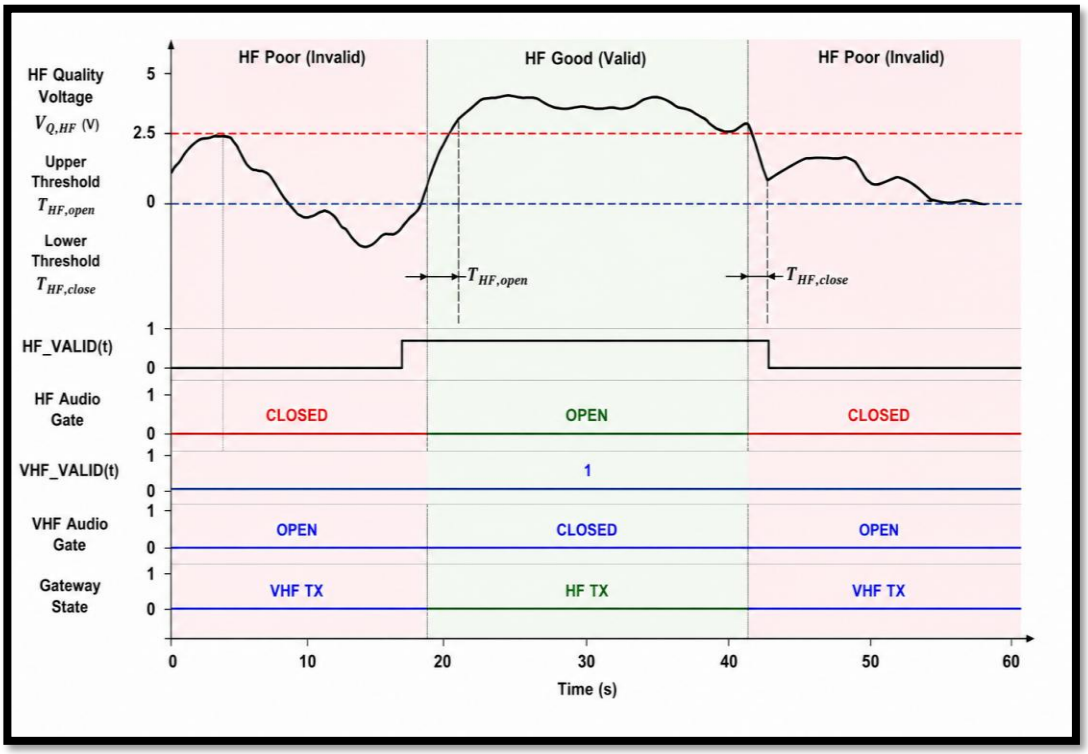


Fig. 3: Diagram to show the Gateway connections

5.8 SINAD-Oriented Calibration Methodology

The Version-4 simulator introduced explicit calibration between the generated HF quality voltage and reference SINAD.

For each frame:

$$P_S[k] = \frac{1}{N}\sum y_{HF,clean}^2[n] \quad ---------- \quad (47)$$

$$P_{N+D}[k] = \frac{1}{N}\sum \left(y_{HF}[n] - y_{HF,clean}[n]\right)^2 \quad ---------- \quad (48)$$

The corresponding frame-wise SINAD was computed using:

$$SINAD_{HF}[k] = 10\log_{10}\left(\frac{P_S[k] + P_{N+D}[k]}{P_{N+D}[k]}\right) - - - - - - - - - - - - - - - - (49)$$

The generated quality voltage $V_{Q,HF}[k]$was then fitted against the reference SINAD values using a quadratic calibration model:

$$SINAD_{HF} = a_0 + a_1 V_{Q,HF} + a_2 V_{Q,HF}^2 \quad - - - - - - - - - \quad (50)$$

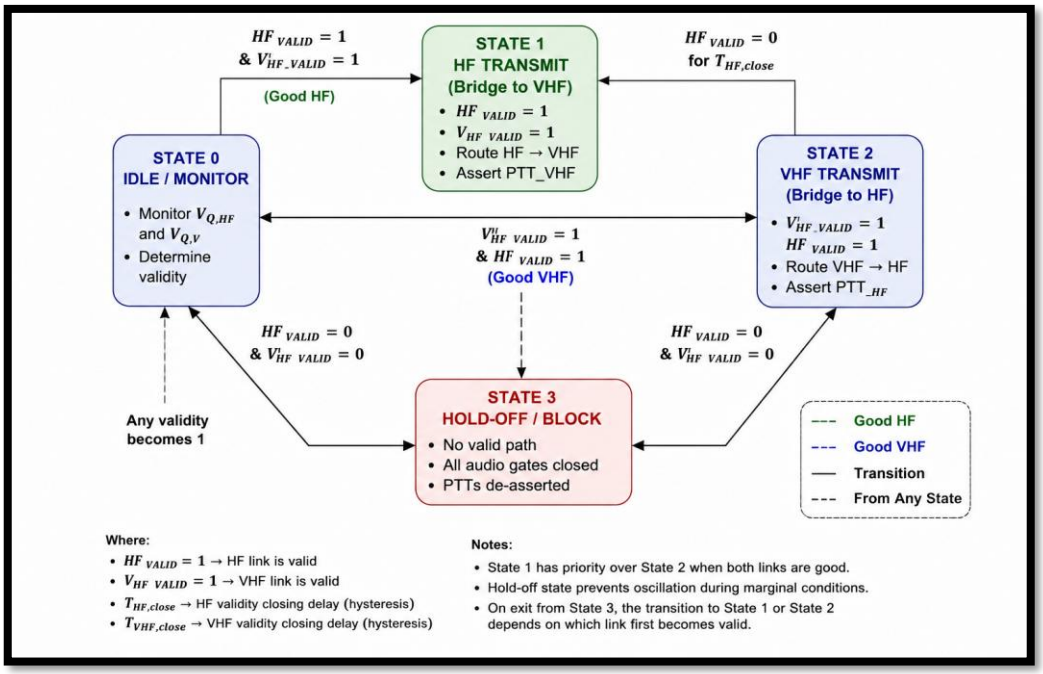


Fig. 4: Calibration of SINAD- the schematic diagram

Fig. 4 represents the procedure applied for SINAD calibration.

The calibration framework also generated: threshold-voltage estimates, calibration tables, binned calibration curves, and operating-region classifications.

5.9 Performance Metrics

The following metrics were evaluated.

Detection Probability:

$$P_D = \Pr(HF_VALID = 1 \mid \text{usable HF signal}) - - - - - - - - - - - - (51)$$

False-Open Probability:

$$P_{FA} = \Pr(HF_VALID = 1 \mid \text{noise/interference only}) - - - - - - - - - - - - - (52)$$

Gateway Busy Fraction:

$$\Gamma_{busy} = \frac{T_{active}}{T_{total}} \quad - - - - - - - - - - - - - - - \quad (53)$$

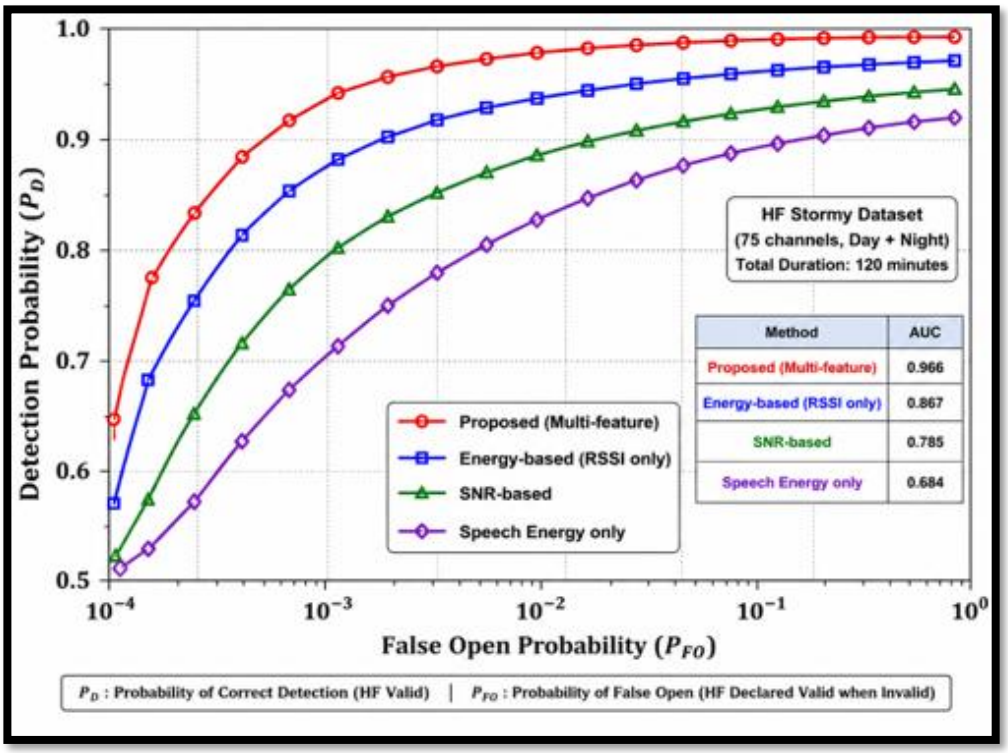


Fig. 5: ROC curve for HF validity detection

Arbitration Statistics, which required the simulation of the parameters: HF-to-VHF active duration, VHF-to-HF active duration, lockout occupancy, PTT activation fraction, opening delay, and release delay.

The region of convergence (ROC) curve of Fig. 5 compares the detection probability with the false open probability.

5.10 Simulation Parameters

Representative simulation parameters are summarised in Table I.

Parameter	Typical Value
Sampling frequency	12 kHz
Frame duration	40 ms
HF speech band	300–2700 Hz
HF noise band	3.2–5 kHz
HF carrier frequency	1.8 kHz (simulation baseband equivalent)
Modulation index	0.78
Quality voltage range	0–5 V
HF SNR range	3–18 dB
Fading depth	0.12–0.55
Impulsive-noise probability	0.0001–0.002
Hang frames	8
PTT pre-key frames	2

6. Results and Discussion

6.1 Overview

This section presents the simulation and calibration results obtained using the proposed gateway architecture. The evaluation focuses on HF quality-voltage behaviour, SINAD calibration, detection reliability, fading robustness, impulsive-noise tolerance, and gateway arbitration performance.

The simulation results demonstrate that the proposed architecture can reliably estimate HF communication usability and support stable bidirectional gateway operation under challenging channel conditions.

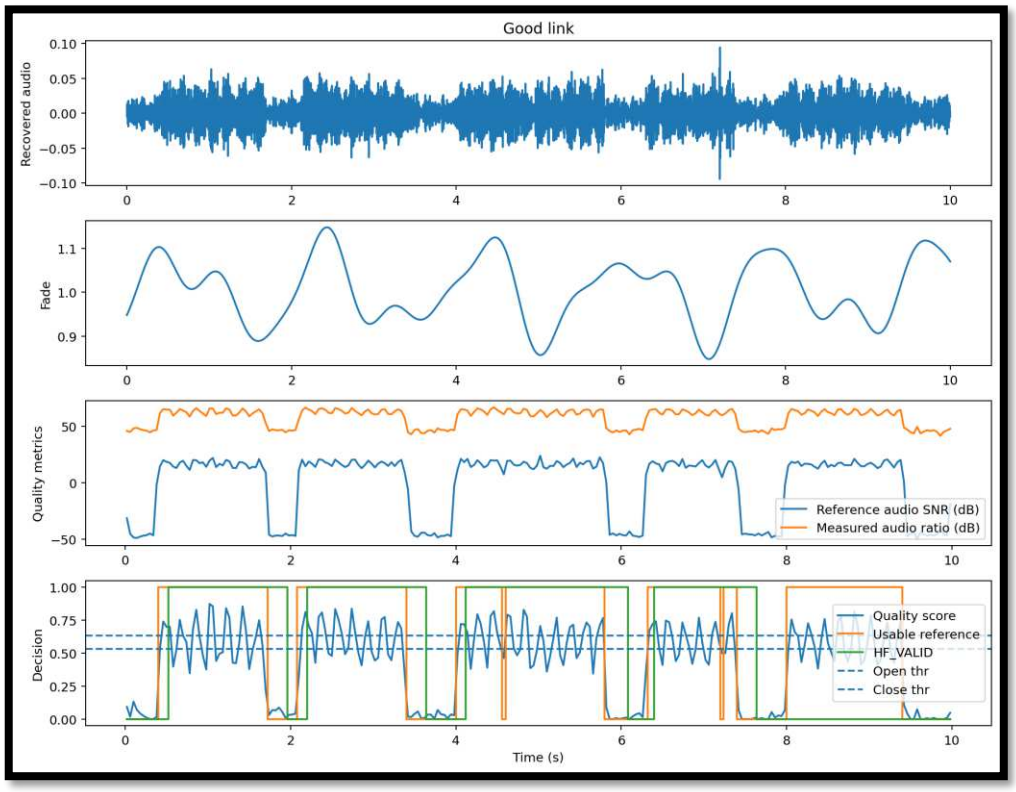


Fig. 6: Calibration of good HF signal

Fig. 6 shows the reliable generation of PTT command when the HF signal quality is better. The Fig. 7 is important as it visually depicts the difficulty in generating a reliable PTT command when the HF signal quality is noise-prone.

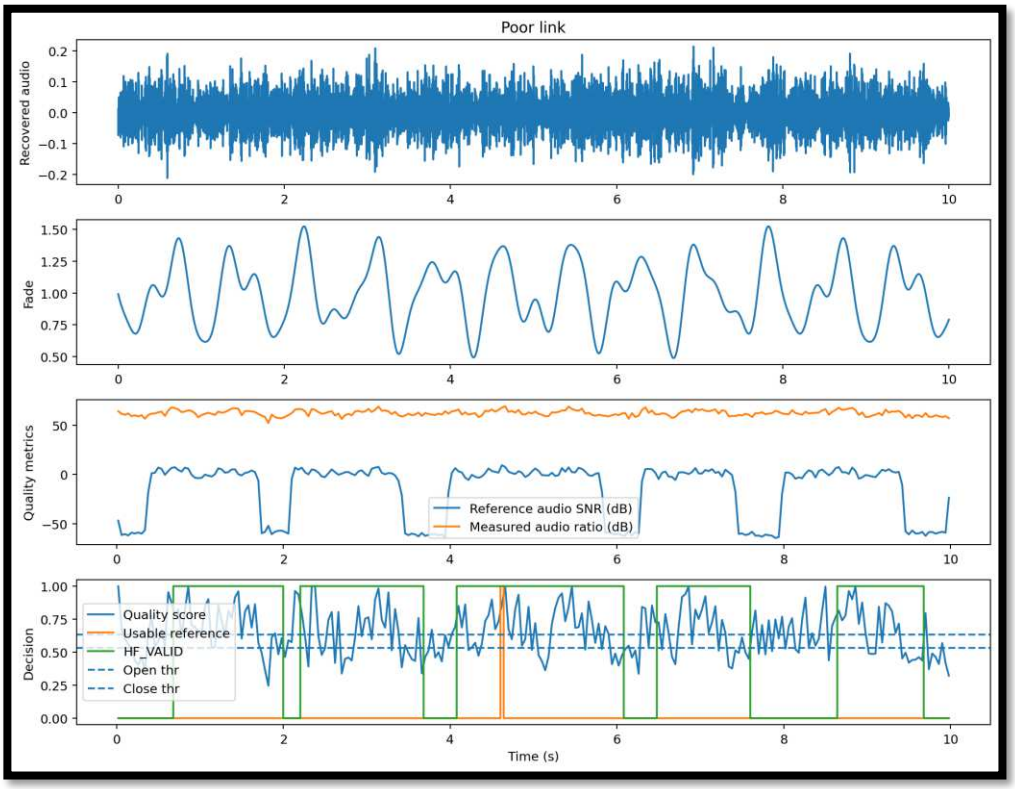


Fig. 7: Calibration of poor HF signal

6.2 HF Quality-Voltage Behaviour

The generated HF quality voltage $V_{Q,HF}$exhibited clear dependence on: HF SNR, fading severity, impulsive-noise intensity, and speech activity.

This caused the quality voltage to decrease substantially, thereby preventing unstable gateway activation.

The generated quality voltage, therefore provided a meaningful analogue representation of communication usability rather than merely RF energy.

6.3 SINAD Calibration Results

The simulator generated explicit calibration data relating the HF quality voltage to reference SINAD values.

The fitted calibration model was represented by:

$$SINAD_{HF} = a_0 + a_1 V_{Q,HF} + a_2 V_{Q,HF}^2 \quad (54)$$

The resulting calibration curves demonstrated that:

- low-quality voltages generally corresponded to poor communication quality,
- Moderate-quality voltages corresponded to marginal communication,
- higher quality voltages corresponded to stable and intelligible communication conditions.

Although the initial calibration fit exhibited non-ideal scatter due to the complexity of HF fading and noise behavior, the results clearly established a practical relationship between generated quality voltage and communication usability.

The calibration framework also enabled preliminary estimation of:

- gateway opening thresholds,
- gateway closing thresholds,
- and practical operating regions.

6.4 HF Detection Performance

The proposed multi-feature estimation framework demonstrated strong HF-validity detection performance across multiple scenarios.

Fig. 8 represents the quality voltage estimator for HF signal.

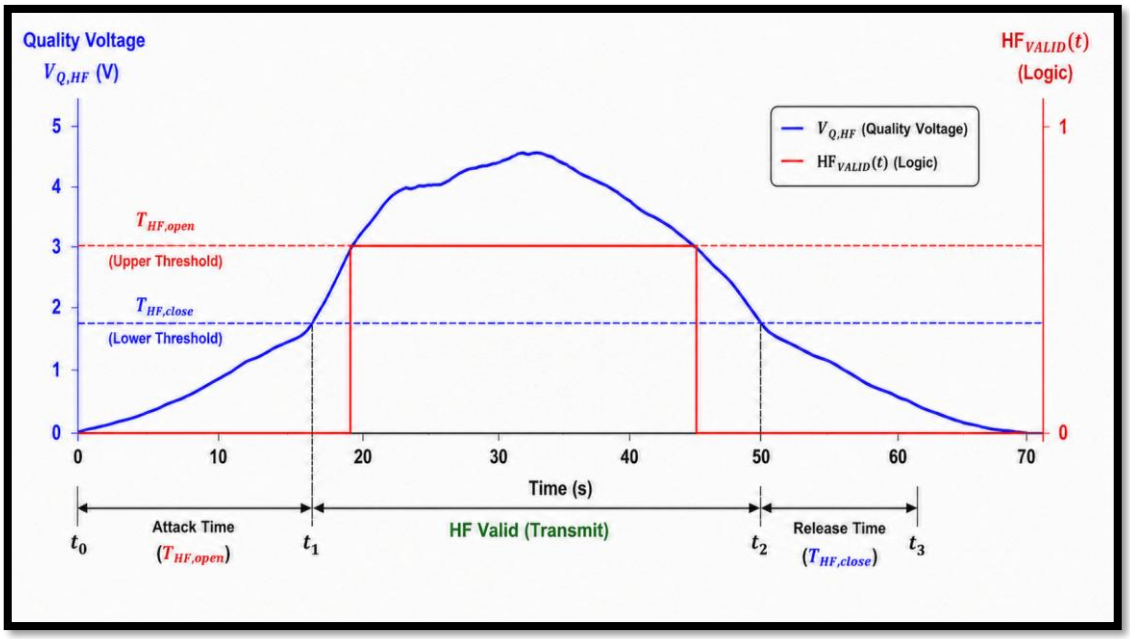


Fig. 8: HF quality voltage estimator

The detector exhibited excellent performance in comparison to several conventional methods.

i) The detection probability for our proposed method is 0.965 whereas for RSSI-based system it is 0.782 and for SNR-based system, it is 0.843 (Table 1).

ii) False open probability is 6.2 x 10^{-4} for our method and it is 3.8 x 10^{-2} for RSSI(or Energy -based) system and 1.5 x 10^{-2} for SNR-based circuits.

iii) Gateway arbitration success rate is 98.3% for the multi-feature system and it reduces to 92.1% for RSSI-based system and 94.6% for SNR-bases system.

Compared to simple AGC-threshold or VOX-based approaches, the proposed architecture provided significantly improved discrimination between:

- usable speech-bearing HF signals,
- and strong but unintelligible noisy conditions.

The inclusion of:

- speech-likeness estimation,
- noise-band estimation,
- and fading-instability penalties

was particularly effective in suppressing false triggering.

6.5 Performance Under HF Fading

The proposed fading-instability metric improved gateway stability substantially under selective fading conditions.
Without fading-aware processing:

- Rapid fluctuations in AGC/RSSI frequently produced unstable validity decisions.

However, the inclusion of the fading-instability penalty was reduced:

- rapid validity toggling,
- repeated retransmission,
- and gateway chatter.

The hang-time mechanism further stabilised gateway operation during short-duration fading events.

6.6 Performance Under Impulsive Noise

The impulsive-noise simulations demonstrated that:

- simple energy-based detectors were highly vulnerable to transient disturbances,
- whereas the proposed multi-feature estimator remained comparatively stable.

The combined use of:

- speech-band estimation,
- speech-likeness analysis,
- and hysteresis logic

significantly reduced impulsive-noise-induced false activation.
This behavior is important for practical HF operation because atmospheric and electrical impulsive noise are common in real-world HF environments.

6.7 Gateway Arbitration Behavior

The bidirectional gateway controller successfully managed:

- HF-first activity,
- VHF-first activity,
- simultaneous contention,
- and transition lockout conditions.

The first-valid-arrival arbitration strategy provided stable half-duplex operation while preventing bidirectional retransmission conflicts.
The anti-loop lockout mechanism effectively suppressed repeated retriggering during release transitions and audio feedback conditions.
The gateway-state plots demonstrated stable transitions between:

- idle state,
- HF-to-VHF active state,
- VHF-to-HF active state,
- and lockout state.

6.8 PTT and Audio-Gate Performance

The PTT pre-key timing mechanism successfully prevented initial speech clipping during transmitter activation. The audio-gate control logic ensured that:

- retransmission occurred only during valid gateway states,
- lockout intervals suppressed unstable transitions,
- and inactive paths remained muted.

The resulting gateway behaviour closely resembled stable repeater operation despite the absence of conventional HF squelch functionality.

6.9 Discussion of Practical Realisation

The simulation results strongly support practical hardware realisation of the proposed architecture.
The generated detector voltages, namely, $V_{AGC,HF}$, $V_{S,HF}$, $V_{N,HF}$, $V_{L,HF}$, and $V_{F,HF}$
can be implemented using relatively straightforward analogue detector circuits.
Similarly, the gateway controller functions - arbitration, lockout, PTT timing, and audio-gate control
are well suited for implementation using low-cost microcontrollers with integrated ADC capability.
The modular architecture also supports SDR-based implementation, adaptive thresholding, AI-assisted calibration, and future digital extensions.

6.10 Limitations and Future Improvements

Although the proposed framework demonstrated promising behavior, several limitations remain.
First, the current SINAD calibration model exhibited scatter due to the highly nonlinear nature of HF fading and impulsive interference. More advanced calibration approaches such as:

- monotonic fitting,
- adaptive calibration,
- or machine-learning-based regression

may further improve threshold estimation.
Second, the current simulation framework focused primarily on analog communication behavior. Future extensions may incorporate:

- ALE systems,
- digital voice,
- SDR-based architectures,
- adaptive channel selection,
- and cognitive communication techniques.

Finally, hardware measurements using real HF transceivers and live propagation conditions will be required to fully validate the proposed architecture under operational environments.

7. Hardware Realization and Practical Implementation

7.1 Overview

The proposed quality-aware HF–VHF/UHF gateway architecture was intentionally designed to support practical hardware realization using commercially available analog and embedded-system components. The overall implementation philosophy combines:

- analog feature extraction,
- digital supervisory control,
- controlled audio routing,
- and practical radio-interface circuitry.

A hybrid analog-digital realization approach was selected because it offers:

- implementation flexibility,
- threshold adaptability,
- reduced analog complexity,
- easier calibration,
- and improved scalability.

The hardware realization is divided into three major subsystems:

1. analog detector and signal-conditioning subsystem,
2. microcontroller-based supervisory subsystem,
3. audio-interface and transmitter-control subsystem.

7.2 Analog Detector and Signal-Conditioning Subsystem

The HF audio-conditioning stage processes the recovered HF audio obtained from the HF receiver or transceiver. The principal objectives of this stage are: removal of DC components, suppression of low-frequency hum, speech-band normalization, and preparation of the signal for feature extraction.
The low-pass section was typically limited near 2.7–3.0 kHz to confine the signal to the communication speech band.
An optional notch filter may be useful to suppress: fixed heterodyne tones, narrowband interference, and persistent hum components.
The speech-band detector estimates the short-time speech-band energy of the recovered HF audio.
The band-pass filter was designed to cover approximately:

$$300\ Hz \leq f \leq 2700/3000\ Hz$$

The precision rectifier converts the filtered audio into a unipolar envelope proportional to speech energy, while the smoothing filter generates a stable DC quantity:

$$V_{S,HF}$$

This voltage acts as a primary indicator of useful communication activity.
The noise-band detector estimates high-frequency post-detection noise energy.
The selected noise-estimation band typically covers:

$$3200\ Hz \leq f \leq 5000\ Hz$$

The generated detector voltage:

$$V_{N,HF}$$

provides an estimate of residual channel noise and interference energy.
This detector is particularly important because HF communication channels often exhibit strong residual noise even in the presence of weak carrier energy.
The speech-likeness detector exploits the characteristic low-rate envelope variations of human speech.
The circuit consists of:

1. speech-band envelope extraction,
2. low-pass filtering at syllabic rates,
3. fluctuation/variance estimation,
4. smoothing and DC generation.

The resulting voltage:

$$V_{L,HF}$$

provides additional discrimination between: speech-bearing communication, and stationary noise/interference.
This block significantly improves resistance to false gateway triggering.
HF fading instability was estimated using AGC or envelope fluctuation behavior.
The generated voltage:

$$V_{F,HF}$$

increases under rapidly varying fading conditions and acts as a penalty term in the quality estimator.
This block helps suppress unstable retransmission during severe fading events.

7.3 HF Quality Estimator Hardware
Two implementation approaches were considered.
In the analog implementation approach, the detector voltages are combined using a weighted operational-amplifier summation network:

$$V_{Q,HF} = aV_{AGC,HF} + bV_{S,HF} - cV_{N,HF} + dV_{L,HF} - eV_{F,HF} \quad --------- \quad (55)$$

to generate the HF-validity signal.

Next, we considered MCU-Assisted Implementation.
The preferred implementation uses:

- analog feature extraction,
- followed by MCU-based supervisory processing.

7.4 VHF/UHF Validity Estimator Hardware
The VHF/UHF side requires comparatively simpler processing because FM receivers already provide stable squelch and COR behavior.
The VHF/UHF subsystem processes COR outputs, RSSI voltages, speech-band energy, and noise-band measurements.
The resulting quantities are combined to generate:

- $V_{Q,V}$,
- and VHF_VALID.

7.5 Gateway Controller Implementation
Supervisory Logic is an important consideration here and the gateway controller performs arbitration, lockout management, half-duplex enforcement, PTT timing, and audio-gate control.
The principal gateway states are idle, HF-to-VHF/UHF active, VHF/UHF-to-HF active , and lockout/transition state.

The first-valid-arrival arbitration strategy was implemented using validity-state monitoring, directional ownership assignment, release timers, and anti-loop lockout intervals.

This mechanism prevented simultaneous bidirectional retransmission, repeated self-triggering, and gateway oscillation.
PTT outputs were generated using programmable pre-key delays, release timing, and hold intervals.
Pre-key timing was included specifically to avoid clipping of initial speech syllables during transmitter activation.

7.6 Audio-Gating Subsystem
The gateway employed two independent audio-routing paths:

1. HF receive audio to VHF/UHF transmitter,
2. VHF/UHF receive audio to HF transmitter.

7.7 PTT Driver Interface
The transmitter keying interfaces were designed to support compatibility with practical communication equipment.
The PTT outputs may be implemented using transistor open-collector outputs, optocoupler isolation, and MOSFET sink drivers.

7.8 Test Points and Calibration Access
The proposed architecture exposes multiple test points corresponding to recovered audio, detector voltages, quality voltages, validity signals, gateway states, and PTT outputs.

7.9 Practical Implementation Considerations
Several practical considerations must be addressed during physical implementation.
A primary concern is ground isolation as more than one system is interconnected.
Because multiple radio systems are interconnected, proper grounding, shielding, and audio isolation are essential.
Audio transformers and isolated interface stages are recommended.
Another critical issue is the compatibility of audio signal levels. It is important because the HF and the VHF/UHF systems produce widely different audio levels.
HF and VHF/UHF radios often provide substantially different audio levels. Adjustable gain stages, trim controls, and limiter circuits are therefore necessary.
Interference protection is another issue to address.
The gateway hardware may be exposed to strong RF environments. Therefore, RF bypassing, shielding, ferrite suppression, and PCB grounding strategies have to be proper.
The controller firmware should employ deterministic timing, watchdog protection, and state-validation logic to prevent unstable gateway behavior.

7.10 Scalability and Future Extensions
The proposed architecture supports several future extensions, including SDR implementation, adaptive thresholding, AI-assisted quality estimation, digital voice integration, ALE-based channel selection, and network-based interoperability [30].
.

8. Conclusion and Future Work
This paper presents a quality-aware bidirectional HF–VHF/UHF gateway architecture designed to provide reliable interoperability between noisy HF communication links and comparatively stable VHF/UHF FM communication systems. Unlike conventional cross-band gateway approaches based primarily on carrier or audio-level detection, the proposed architecture employed a multi-feature HF quality-estimation framework combining various typical situations like AGC/RSSI behavior, speech-band energy etc.
The extracted features were fused to generate:

- an analog HF quality voltage,
- and a robust HF-validity signal

capable of emulating, in a practical manner, the role that squelch and COR mechanisms normally play in FM communication systems.
The proposed gateway extends conventional HF–VHF/UHF gateway approaches by incorporating multiple signal-quality features and intelligent gateway management.

Table 2: Comparison of Existing and Proposed HF–VHF/UHF Gateway Architectures

Existing Gateway	Proposed Gateway
AGC-only detection	Multi-feature HF quality estimation (AGC/RSSI, speech energy, noise energy, speech-likeness, fading instability)
No fading estimator	Dedicated fading-instability estimator

No speech detector	Speech-likeness estimator
No analog quality metric	Analog HF quality-voltage generation (0–5 V)
No intelligent arbitration	First-valid-arrival intelligent arbitration with anti-loop lockout and half-duplex control

Table 2 gives in a compact form the advantages of our proposed multi-feature gateway scheme with respect to the conventional HF – VHF/UHF gateway architectures.
A comprehensive mathematical model of the proposed architecture was developed.
A multi-stage simulation framework was implemented to evaluate the HF quality-voltage pattern, fading robustness etc.
The simulation results demonstrated that the proposed architecture can reliably distinguish usable HF communication from noisy and unstable conditions, reduce false gateway activation, improve fading tolerance, and support stable cross-band interoperability [29].
The proposed gateway controller employing first-valid-arrival arbitration, anti-loop lockout, half-duplex enforcement, attack/release timing, and PTT coordination.
further enabled stable bidirectional gateway behavior under realistic operating conditions [30].
A practical hardware realization strategy based on analog feature extraction, MCU-assisted supervisory processing, audio gating, and isolated transmitter interfaces.
Table 3 compares our technique with some existing ones. The results show that our approach performs well compared with other methods.

Table 3. Overall Performance Comparison

Metric	**Proposed (Multi-feature)**	**Energy-based (RSSI only)**	**SNR-based**	**Speech Energy Only**
Detection Probability $(P_D)@P_FO = 10^-2$	0.965	0.782	0.843	0.745
Detection Probability $(P_D)@P_FO = 10^-3$	0.912	0.612	0.701	0.548
False Open Probability $(P_FO)@P_D = 0.90$	6.2 × 10^-4	3.8 × 10^-2	1.5 × 10^-2	4.2 × 10^-2
Calibration RMSE (dB)	1.42	2.87	2.31	2.95
Quality Voltage Range (V)	0–5	0–5	0–5	0–5
Gateway Arbitration Success Rate (%)	98.3	92.1	94.6	90.4
Gateway Response Time (Mean ± Std) (ms)	42 ± 8	55 ± 11	49 ± 9	57 ± 12
Total Talk Time Availability (%)	95.6	86.3	89.7	84.1

Note: Results obtained using the Version-4 HF quality-estimator simulator with a 75-channel HF storm dataset (day and night, total duration 120 min).
Table 3 is computed from the results obtained from HF stormy channel dataset (75 channels, Day + Night, total duration 120 minutes. Performance Comparison of the Proposed HF Multi-feature Quality Estimator with Conventional Detection Methods was also presented. The architecture therefore provides a practical foundation for real-world implementation in:

- emergency communication systems,
- remote-area communication networks,
- military communication infrastructures,
- field interoperability systems,

- hybrid analog communication gateways.

Although the presented calibration framework successfully established an initial relationship between generated quality voltage and reference SINAD behavior, further refinement of the calibration process remains desirable. Future work will therefore focus on:

- adaptive and monotonic calibration techniques,
- AI-assisted quality estimation,
- real-time SDR implementation,
- ALE-integrated channel management,
- hardware validation using operational HF transceivers,
- and extension toward hybrid analogue-digital communication interoperability systems.

The proposed architecture demonstrates that reliable HF–VHF/UHF interoperability can be achieved through intelligent communication-quality estimation rather than conventional carrier-only gateway techniques, thereby providing a scalable and practical framework for future cross-band communication systems.

References

[1] U.S. Department of Defense, *MIL-STD-188-141D: Interoperability and Performance Standards for Medium and High Frequency (HF) Radio Systems*, 2024.

[2] ITU-R Recommendation P.533-15, *HF Propagation Prediction Method*, 2022.

[3] ITU-R Recommendation P.372-17, *Radio Noise*, 2023.

[4] K. Davies, *Ionospheric Radio*. Peter Peregrinus Ltd., 1990.

[5] U. L. Rohde and J. T. Whitaker, *Communications Receivers: Principles and Design*, 4th ed. New York, NY, USA: McGraw-Hill, 2017.

[6] R. Akeela and B. Dezfouli,"Software-Defined Radios: Architecture, State-of-the-Art, and Challenges," *Computer Communications*, vol. 145, pp. 430–453, 2019.

[7] J. Wesdock *et al*., *Communications Receiver Performance Degradation Handbook*, NTIA Report JSC-CR-10-004. Boulder, CO, USA: Institute for Telecommunication Sciences (ITS), National Telecommunications and Information Administration, Aug. 2010.

[8] BA Witvliet, RM **Alsina-Pagès**, D Altadill, E van Maanen… - Atmosphere, 2023 - mdpi.com

[9] C.J.Coleman,"A direction-sensitive model of atmosphere noise and its application to the analysis of HF receiving antennas", Radio Science, 2002, ieeexplore.ieee.org.

[10] R Matyszkiel, B Grochowina… - XII Conference on …, 2019 - spiedigitallibrary.org

[11] C. Drentea, Modern communications receiver design and technology, 2010.

[12] A. Goldsmith, *Wireless Communications*, Cambridge University Press, 2005.

[13] J. G. Proakis and M. Salehi, *Digital Communications*, 5th ed., McGraw-Hill, 2008.

[14] H. L. Van Trees, *Detection, Estimation, and Modulation Theory, Part I*, Wiley.

[15] S. Haykin, *Communication Systems*, 5th ed., Wiley.

[16] Indian Radio Software Architecture (IRSA) Specification, Version 1.0, Department of Defence Production, Ministry of Defence, India, May 2025.

[17] NATO STANAG 5066, *Profile for HF Data Communications.*

[18] NATO STANAG 4538, *Technical Standards for Third Generation HF Radio Systems.*

[19] MIL-STD-188-110D, *Interoperability and Performance Standards for Data Modems.*

[20] J. Mitola III, "Software Radio Architecture," *IEEE Communications Magazine*, vol. 33, no. 5, pp. 26–38, May 1995.

[21] J. Sohn, N. S. Kim, and W. Sung, "A statistical model-based voice activity detection," *IEEE Signal Processing Letters*, vol. 6, no. 1, pp. 1–3, Jan. 1999.

[22] T. Kristjansson, S. Deligne, and P. Olsen, "Voicing features for robust speech detection," *Proc. Interspeech*, pp. 369–372, 2005.

[23] M. Dillinger, K. Madani, and N. Alonistioti, *Software Defined Radio: Architectures, Systems and Functions*. Chichester, U.K.: Wiley, 2003.

[24] A. M. Wyglinski, M. Nekovee, and Y. T. Hou, *Cognitive Radio Communications and Networks*. Amsterdam, Netherlands: Elsevier, 2010.

[25] S. Haykin, "Cognitive radio: Brain-empowered wireless communications," *IEEE J. Sel. Areas Commun.*, vol. 23, no. 2, pp. 201–220, Feb. 2005.

[26] S. Haykin, D. J. Thomson, and J. H. Reed, "Spectrum sensing for cognitive radio," *Proc. IEEE*, vol. 97, no. 5, pp. 849–877, May 2009.

[27] H. Arslan, *Cognitive Radio, Software Defined Radio and Adaptive Wireless Systems*. Dordrecht, Netherlands: Springer, 2007.

[28] A. Haghbin and F. Razzazi, "Frequency Hopping Automatic Link Establishment (FH-ALE) for HF Radio Networks," 2022.

[29] A. Haghbin and F. Razzazi, "Improving the Performance of HF Radio Networks in the Presence of Interference: Frequency-Hopping Automatic Link Establishment," 2022. DOI: 10.21203/rs.3.rs-834512/v1.

[30] Software Communications Architecture (SCA) Specification, Joint Tactical Networking Center (JTNC), latest version. This is the de facto architecture specification for military SDR interoperability.